Soft Matter

www.rsc.org/softmatter

Volume 8 | Number 34 | 14 September 2012 | Pages 8797–9030

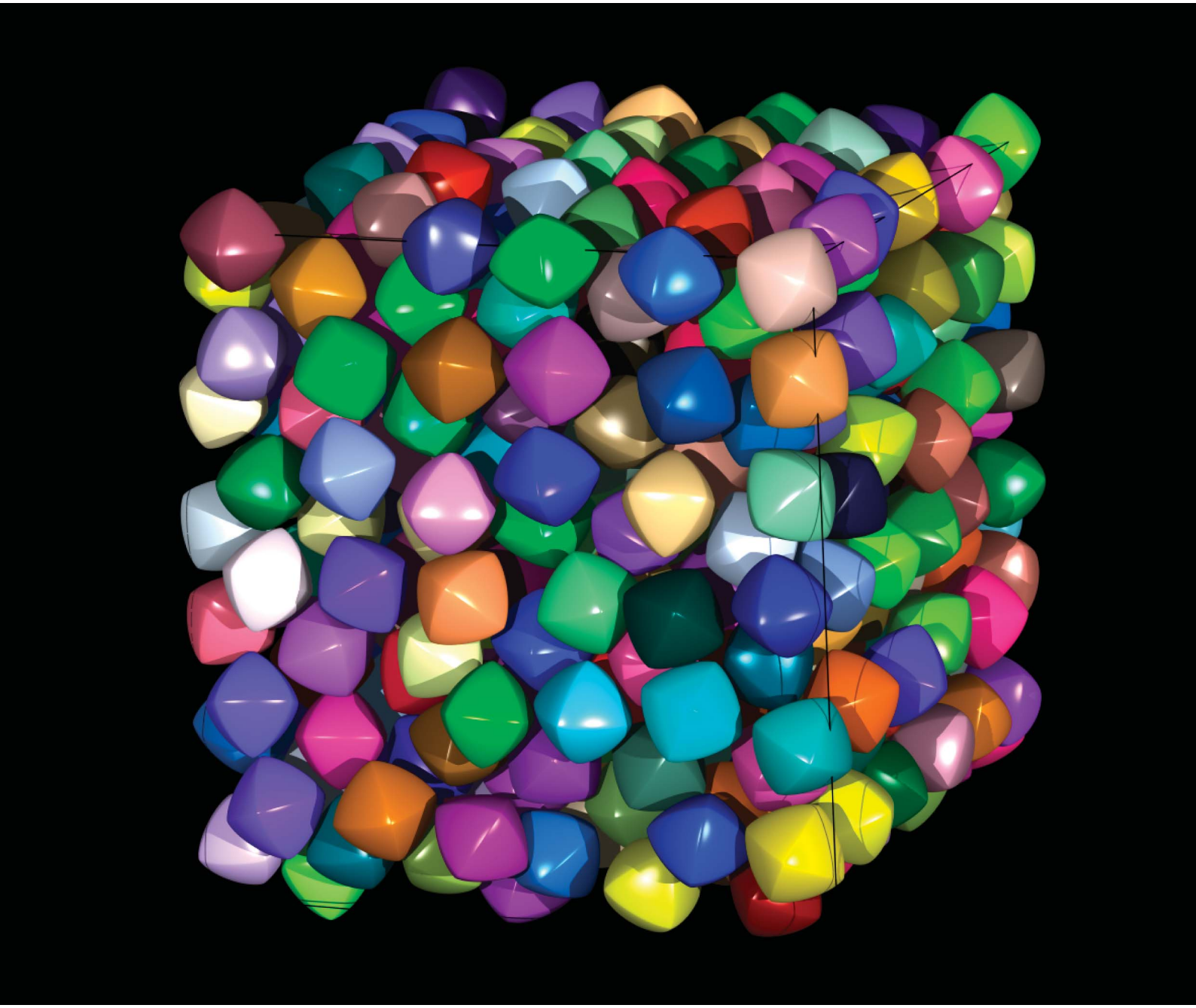

ISSN 1744-683X

RSC Publishing

PAPER

Ran Ni, Marjolein Dijkstra *et al.*

Phase diagram of colloidal hard superballs: from cubes *via* spheres to octahedra

1744-683X(2012)8:34;1-7

Soft Matter

Dynamic Article Links

Cite this: *Soft Matter*, 2012, **8**, 8826

www.rsc.org/softmatter

PAPER

Phase diagram of colloidal hard superballs: from cubes *via* spheres to octahedra†

Ran Ni,*[a] Anjan Prasad Gantapara,[a] Joost de Graaf,[a] René van Roij[b] and Marjolein Dijkstra*[a]

Received 6th April 2012, Accepted 1st June 2012
DOI: 10.1039/c2sm25813g

For hard anisotropic particles the formation of a wide variety of fascinating crystal and liquid-crystal phases is accomplished by entropy alone. A better understanding of these entropy-driven phase transitions will shed light on the self-assembly of nanoparticles, however, there are still many open questions in this regard. In this work, we use Monte Carlo simulations and free-energy calculations to determine the phase diagram of colloidal hard superballs, of which the shape interpolates between cubes and octahedra *via* spheres. We discover not only a stable face-centered cubic (fcc) plastic crystal phase for near-spherical particles, but also a stable body-centered cubic (bcc) plastic crystal close to the octahedron shape. Moreover, coexistence of these two plastic crystals is observed with a substantial density gap. The plastic fcc and bcc crystals are, however, both unstable in the cube and octahedron limit, suggesting that the local curvature, *i.e.* rounded corners and curved faces, of superballs plays an important role in stabilizing the rotator phases. In addition, we observe a two-step melting phenomenon for hard octahedra, in which the Minkowski crystal melts into a metastable bcc plastic crystal before melting into the fluid phase.

1. Introduction

Recent breakthroughs in particle synthesis have resulted in a spectacular variety of anisotropic nanoparticles such as cubes, octapods, tetrapods, octahedra, ice cones, *etc.*[1] A natural starting point to study the self-assembled structures of these colloidal building blocks is to view them as hard particles.[1] Not only can these hard-particle models be used to predict properties of suitable experimental systems, but such models also provide a stepping stone towards systems where soft interactions play a role.[2,3] Moreover, the analysis of hard particles is of fundamental relevance and raises problems that influence fields as diverse as (soft) condensed matter,[1,4–6] mathematics,[5,7] and computer science.[8] In this light the concurrent boom in simulation studies of hard anisotropic particles is not surprising.[5–7,9–17]

The best-known hard-particle system consists of hard spheres, which freeze into close-packed hexagonal (cph) crystal structures,[8] of which the ABC-stacked cph crystal, better known as the face-centered cubic (fcc) crystal phase, is thermodynamically stable.[18] Hard anisotropic particles can form liquid-crystalline equilibrium states if they are sufficiently rod- or disclike,[13,17] but particles with shapes that are close-to-spherical tend to order into plastic crystal phases, also known as rotator phases.[15–17] In fact, simple guidelines were recently proposed to predict the plastic- and liquid-crystal formation only on the basis of rotational symmetry and shape anisotropy of hard polyhedra.[6,19] In this work we will take a different approach, based on free-energy calculations, and address the question whether and to what extent rounding the corners and faces of polyhedral particles affects the phase behavior. Such curvature effects are of direct relevance to experimental systems, in which sterically and charged stabilised particles can often *not* be considered as perfectly flat-faced and sharp-edged.[20] For instance, recent experiments on nanocube assemblies show a continuous phase transformation between simple cubic and rhombohedral phases by increasing the ligand thickness and hence the particle sphericity.[3]

In this paper, we study a system of colloidal hard superballs in order to address these problems. A superball is defined by the inequality

$$|x|^{2q} + |y|^{2q} + |z|^{2q} \leq 1, \quad (1)$$

where x, y and z are scaled Cartesian coordinates with q the deformation parameter, and we use radius a of the particle as our unit of length. The shape of the superball interpolates smoothly between two Platonic solids, namely the octahedron ($q = 0.5$) and the cube ($q = \infty$) *via* the sphere ($q = 1$) as shown in Fig. 1. We define the asphericity as

[a]*Soft Condensed Matter, Utrecht University, Princetonplein 5, 3584 CC Utrecht, The Netherlands. E-mail: r.ni@uu.nl; m.dijkstra1@uu.nl; Fax: +31 30 2532706; Tel: +31 30 2533270*
[b]*Institute for Theoretical Physics, Utrecht University, Leuvenlaan 4, 3584 CE Utrecht, The Netherlands*

† Electronic supplementary information (ESI) available: a movie of a plastic bcc crystal formed by superballs with $q = 0.7$ at packing fraction 0.54. See DOI: 10.1039/c2sm25813g

$$A = 1 - \frac{\pi^{1/3}[6v(q)]^{2/3}}{S(q)}, \tag{2}$$

where $S(q)$ is the surface area of the particle. The volume of the superball $v(q)$ is given by

$$v(q) = 8a^3 \int_0^1 \int_0^{\left(1-x^{2q}\right)^{1/2q}} \left(1 - x^{2q} - y^{2q}\right)^{1/2q} \mathrm{d}y\, \mathrm{d}x$$
$$= \frac{8a^3\left[\Gamma(1+1/2q)\right]^3}{\Gamma(1+3/2q)}, \tag{3}$$

where $a = 1$ is the radius of the particle. This is similar to the definition in ref. 21 and 22. In our definition $A = 0$ for a sphere and $A > 0$ for nonspherical objects. The asphericity increases smoothly and substantially by letting q deviate from $q = 1$. The asphericity of superballs as a function of $1/q$ is shown in Fig. 1. By determining the phase diagram of these superballs as a function of q, we discovered a thermodynamically stable body-centered cubic (bcc) plastic crystal phase for octahedron-like superballs. To the best of our knowledge *no* thermodynamically stable plastic crystals other than cph structures have so far been observed for hard particles. A bcc rotator phase has also recently been reported in simulations of truncated and perfect octahedra parallel to our work.[19] However, the thermodynamical stability of the bcc rotator phase has not been examined in ref. 19. Moreover, we demonstrate using free-energy calculations that bcc and fcc plastic crystal phases are unstable for hard octahedra and hard cubes, respectively. Therefore, rounded faces and edges may play an important role in stabilizing rotator phases, while flat faces tend to stabilize crystals.

The remainder of this paper is organized as follows. We first give a description on the methods we employ to calculate the free energies in Section 2. The phase diagram of the cube-like and octahedron-like superballs is presented in Section 3. Finally, conclusions are drawn in Section 4.

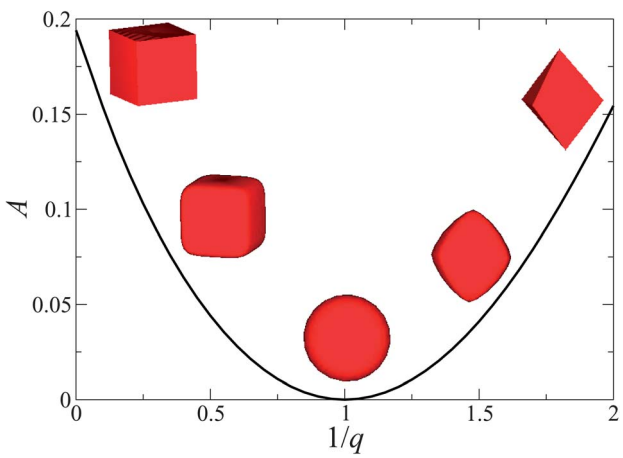

Fig. 1 The asphericity A as a function of $1/q$, where the shape of superballs interpolates between octahedra ($q = 0.5$) and cubes ($q = \infty$) *via* spheres ($q = 1$).

2. Free-energy calculations

2.1. Fluid phase

We employ standard NPT Monte Carlo simulations to obtain the equation of state (EOS) for the fluid phase. For these simulations we use the hard-particle overlap algorithm described in Appendix A.1. We also determine the free energy by integrating the EOS from reference density ρ_0 to ρ:

$$\frac{F(\rho)}{N} = \frac{F(\rho_0)}{N} + \int_{\rho_0}^{\rho} \frac{P(\rho')}{\rho'^2}\mathrm{d}\rho'. \tag{4}$$

Here $F(\rho_0)/N = \mu(\rho_0) - P(\rho_0)/\rho_0$ is the Helmholtz free energy per particle at density ρ_0, with N the number of particles and $\mu(\rho_0)$ the chemical potential, which is calculated by the Widom's particle insertion method.[23]

2.2. Crystal phases

For the free energy of a crystal we use the Einstein integration method. The Helmholtz free energy F of a crystal is

$$F(N,V,T) = F_{\mathrm{Einst}}(N,V,T) - \int_0^{\lambda_{\max}} \mathrm{d}\lambda \left\langle \frac{\partial U_{\mathrm{Einst}}(\lambda)}{\partial\lambda} \right\rangle, \tag{5}$$

where V and T are the volume and temperature of the system, respectively, with k_{B} the Boltzmann constant. F_{Einst} is the free energy of the ideal Einstein crystal given by

$$\frac{F_{\mathrm{Einst}}(N,V,T)}{k_{\mathrm{B}}T} = -\frac{3(N-1)}{2}\ln\left(\frac{\pi k_{\mathrm{B}}T}{\lambda_{\max}}\right) + N\ln\left(\frac{\Lambda_{\mathrm{t}}{}^3\Lambda_{\mathrm{r}}}{\sigma^4}\right)$$
$$+ \ln\left(\frac{\sigma^3}{VN^{1/2}}\right) - \ln\left\{\frac{1}{8\pi^2}\int \mathrm{d}\theta\,\sin(\theta)\mathrm{d}\phi\,\mathrm{d}\chi \right.$$
$$\left. \times \exp\left[-\frac{\lambda_{\max}}{k_{\mathrm{B}}T}\left(\sin^2\psi_{ia} + \sin^2\psi_{ib}\right)\right]\right\}, \tag{6}$$

and

$$U_{\mathrm{Einst}}(\lambda) = \lambda\sum_{i=1}^{N}\left[(\boldsymbol{r}_i - \boldsymbol{r}_{i,0})^2/\sigma^2 + \left(\sin^2\psi_{ia} + \sin^2\psi_{ib}\right)\right], \tag{7}$$

is the aligning potential for fixing the particles onto a crystal lattice, where $(\boldsymbol{r}_i - \boldsymbol{r}_{i,0})$ is the displacement of particle i from its rest position in the ideal Einstein crystal. Here σ is the unit of length, and we use $\sigma = a = 1$ in the free-energy calculation of superballs and $\sigma = v^{1/3}$ in the free-energy calculation of hard octahedra. The angles ψ_{ia} and ψ_{ib} are the minimum angles formed by the two field vectors, *i.e.* $\boldsymbol{a}$ and $\boldsymbol{b}$, in the ideal Einstein crystal and the vectors defining the orientation of the particle in the crystal. Λ_{t} and Λ_{r} in eqn (6) are the translational and orientational thermal wavelengths of the particles, respectively, and both are set to 1.

2.3. Plastic crystal phases

For the free-energy calculations of a plastic crystal phase, we use a soft interaction potential between the particles

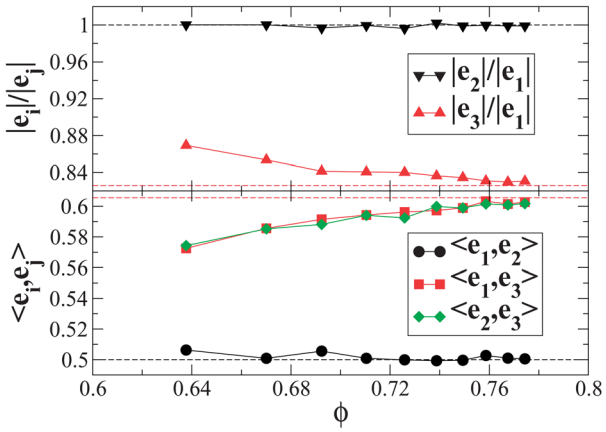

Fig. 2 The deformation of the crystal unit cell with lattice vectors $\boldsymbol{e}_i$ as a function of packing fraction ϕ in a system of hard superballs with $q = 2.5$. The dashed lines in the figures indicate the values for the C_1 crystal.

$$\varphi(i,j) = \begin{cases} \gamma\left[1 - A\left(1 + \zeta(i,j)\right)\right] & \zeta(i,j) < 0 \\ 0 & \text{otherwise} \end{cases}, \tag{8}$$

where $\zeta(i,j)$ is the overlapping potential as defined in ref. 24 which is negative when particles i and j are overlapping and positive otherwise,[24] and γ is the integration parameter with the constant $A = 0.9$.[25] This method was introduced in ref. 25, and allows us to change gradually from a non-interacting system, *i.e.*, $\gamma = 0$, to a plastic crystal phase of hard superballs where $\gamma = \gamma_{\max}$. The Helmholtz free energy of the plastic crystal is then given by

$$F(N,V,T) = F_{\text{Einst}}(N,V,T) - \int_0^{\lambda_{\max}} \mathrm{d}\lambda \left\langle \frac{\partial U_{\text{Einst}}(\lambda)}{\partial \lambda} \right\rangle_{\gamma_{\max}} + \int_0^{\gamma_{\max}} \mathrm{d}\gamma \left\langle \frac{\partial \sum_{i \neq j}^{N} \varphi(i,j)}{\partial \gamma} \right\rangle_{\lambda_{\max}}. \tag{9}$$

3. Results and discussion

3.1. Cube-like superballs ($1 < q < \infty$)

Following ref. 9 and 26, we first calculate the close-packed structures for systems of hard superballs. We employ the algorithm to check for particle overlap as described in Appendix A.1. For cube-like particles, it is found that at close packing there are so-called C_0 and C_1 crystal phases in accordance with ref. 10 and 11. C_0 and C_1 crystals are deformed fcc and simple cubic crystals, respectively, depending on the shape parameter q. We perform NPT Monte Carlo simulations with variable box shape and fixed pressure P, number of particles N, and temperature T to determine the equation of state (EOS) of the crystal phase. Our simulation results show that both the C_0 and the C_1 crystals deform with decreasing density. The lattice vectors for C_0 crystals are given by $\boldsymbol{e}_1 = 2^{1-1/2q}\boldsymbol{i} + 2^{1-1/2q}\boldsymbol{j}$, $\boldsymbol{e}_2 = 2\boldsymbol{k}$, and $\boldsymbol{e}_3 = -2s\boldsymbol{i} + 2(s + 2^{-1/2q})\boldsymbol{j} + \boldsymbol{k}$, where $\boldsymbol{i}$, $\boldsymbol{j}$ and $\boldsymbol{k}$ are the unit vectors along the axes of the particle, and s is the smallest positive root of the equation $(s + 2^{-1/2q})^{2q} + s^{2q} + 2^{-2q} - 1 = 0$. The lattice vectors for C_1 crystals are given by $\boldsymbol{e}_1 = 2^{1-1/2q}\boldsymbol{i} + 2^{1-1/2q}\boldsymbol{j}$, $\boldsymbol{e}_2 = 2^{1-1/2q}\boldsymbol{i} + 2^{1-1/2q}\boldsymbol{k}$, $\boldsymbol{e}_3 = 2(s + 2^{-1/2q})\boldsymbol{i} - 2s\boldsymbol{j} - 2s\boldsymbol{k}$, where s is the smallest positive root of the equation $(s + 2^{-1/2q})^{2q} + 2s^{2q} - 1 = 0$, and there is only one particle in the unit cell.[10,11] For instance, in a C_1 crystal of superballs with $q = 2.5$, one finds that $\langle \boldsymbol{e}_1,\boldsymbol{e}_2 \rangle = 0.5$, $\langle \boldsymbol{e}_1,\boldsymbol{e}_3 \rangle = \langle \boldsymbol{e}_3,\boldsymbol{e}_2 \rangle = 0.60552$, $|\boldsymbol{e}_2|/|\boldsymbol{e}_1| = 1$, and $|\boldsymbol{e}_3|/|\boldsymbol{e}_1| = 0.825737$, where $\langle \boldsymbol{e}_i,\boldsymbol{e}_j \rangle$ is the cosine of the angle between $\boldsymbol{e}_i$ and $\boldsymbol{e}_j$. The calculated angles and the length ratios between lattice vectors as a function of packing fraction ϕ for the cube-like particles with $q = 2.5$ are shown in Fig. 2. We find that at packing fractions approaching close packing, the crystal remains in the C_1 phase. With decreasing packing fraction, the crystal lattice deforms towards a fcc structure: $\langle \boldsymbol{e}_1,\boldsymbol{e}_2 \rangle = \langle \boldsymbol{e}_1,\boldsymbol{e}_3 \rangle = \langle \boldsymbol{e}_2,\boldsymbol{e}_3 \rangle = 0.5$ and $|\boldsymbol{e}_2|/|\boldsymbol{e}_1| = |\boldsymbol{e}_3|/|\boldsymbol{e}_1| = 1$.

Moreover, when $1 < q < 3$, it is found that the deformed C_0 and deformed C_1 crystals melt into a fcc plastic crystal phase. By Einstein integration, we calculated the Helmholtz free energy as a function of packing fraction for both the fcc plastic crystal and the deformed C_1/C_0 crystal phases.[23] Combined with the free-energy calculations for the fluid phase done by Widom's particle insertion method, we obtain the phase boundaries in the phase diagram shown in Fig. 3. Also see Tables 1 and 2 in Appendix A.2 for several values of the free energies used to construct this phase diagram. The part of the phase diagram for hard cube-like superballs roughly agrees with the empirical phase diagram by Batten *et al.*[12] At high packing fractions, there are stable deformed C_0 and C_1 phases. When $q > 1.1509$, the close-packed structure is the C_1 crystal, whereas it is the C_0 crystal whenever $1 < q < 1.1509$.[10,11] To determine the location of the transition from the deformed C_0 crystal to the deformed C_1 crystal, we performed two series of NPT MC simulations with an increasing value of q for the first series and decreasing q for the second series of simulations at pressure $P^* = Pv/k_BT \simeq 250$, with v the volume of the particle.[13] The first series started from a C_0 crystal phase, while the second series of simulations started from a C_1 crystal phase. Our simulations show that the phase transition occurred around $q = 1.09$ at packing fraction $\phi = 0.736$ as shown by the asterisk in Fig. 3. Moreover, for hard cubes ($q = \infty$) the C_1 crystal is a simple cubic (sc) crystal. Although it was found that for hard cubes there is a significant number of vacancies in the simple cubic crystal, it only shifts the phase boundary by ~2% in the packing fraction.[14] In our simulations, we did not observe any vacancies in the crystals of hard superballs with $q \leq 3$, we therefore assume that the possible presence of vacancies would not shift the phase boundary significantly.

3.2. Octahedron-like superballs ($0.5 \leq q < 1$)

The other part of the phase diagram concerns the octahedron-like superballs. For $0.79248 < q < 1$, we obtained a denser structure than the predicted O_0 lattice of ref. 10 and 11. For instance, after compressing the system to pressures around $P^* = 10^7$ at $q = 0.85$, we obtained a body-centered-tetragonal (bct) crystal with $\phi = 0.7661$. This is denser than the O_0 crystal, which achieves $\phi = 0.7656$ at $q = 0.85$. Note, however, that these two crystals are very similar to each other, since O_0 is also a form of a bct lattice. The only difference is that the orientation of the particles in the O_0 crystal is the same as the symmetry of the axes in the crystal lattice, while in our bct crystal there is a small angle between these two orientations in the square plane of the crystal. Furthermore, for $q < 0.79248$, we also found a crystal with denser

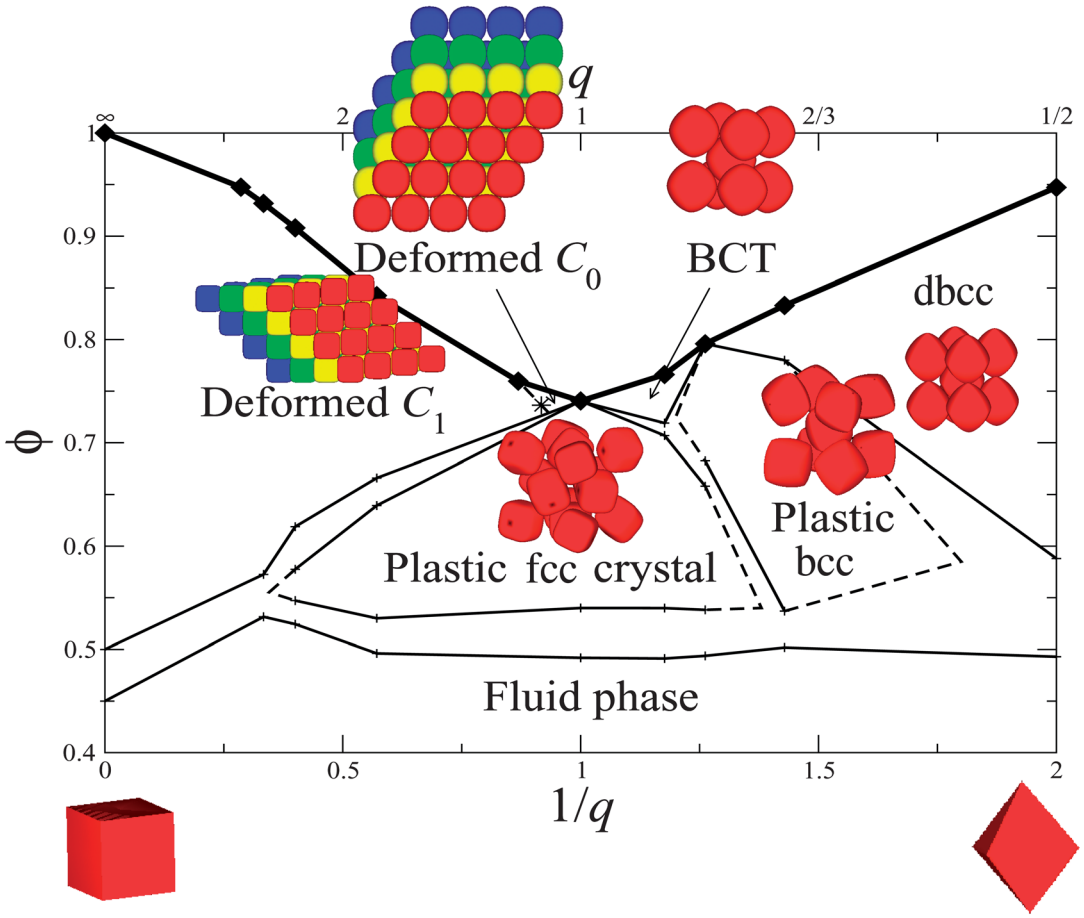

Fig. 3 Phase diagram for hard superballs in the ϕ (packing fraction) *versus* $1/q$ (bottom axis) and q (top axis) representation where q is the deformation parameter. Here the C_1 and C_0 crystals are defined in the main text and in ref. 10 and 11, where the particles of the same color are in the same layer of stacking. The solid diamonds indicate the close packing, and the locations of triple points are determined by extrapolation as shown by the dashed lines. The phase boundaries for hard cubes are taken from ref. 14.

Table 1 Helmholtz free energy per particle, $F(\rho_0)/Nk_BT$, and the chemical potential, $\mu(\rho_0)$, in the fluid phase for several choices of the shape parameter q at density ρ_0. This result was obtained by the Widom particle-insertion method for N particles in the simulation box

q	$\rho_0 a^3$	N	$\mu(\rho_0)/k_BT$	$F(\rho_0)/Nk_BT$
0.70000	0.100	500	1.85523	−1.63213
0.79248	0.100	500	3.32035	−1.14744
0.85000	0.050	500	−0.94569	−3.07702
1.75000	0.020	500	−2.56824	−4.29418
2.50000	0.036	500	0.71808	−2.69570
3.00000	0.028	500	−0.60904	−3.30777

packing than the predicted O_1 crystal in ref. 10 and 11. For $q = 0.7$, we performed floppy-box MC simulations with several particles to compress the system to a high pressure state, *i.e.*, $P^* = 10^7$. We found a deformed bcc (dbcc) crystal shown in Fig. 3, which is an intermediate form between the bcc lattice and the Minkowski crystal.[27] The lattice vectors are $\boldsymbol{e}_1 = 0.912909\boldsymbol{i} + 0.912403\boldsymbol{j} - 0.912165\boldsymbol{k}$, $\boldsymbol{e}_2 = -0.271668\boldsymbol{i} + 1.80916\boldsymbol{j} - 0.288051\boldsymbol{k}$, and $\boldsymbol{e}_3 = 0.28834\boldsymbol{i} - 0.272001\boldsymbol{j} - 1.80882\boldsymbol{k}$, where $\boldsymbol{i}$, $\boldsymbol{j}$, and $\boldsymbol{k}$ are the unit vectors along the axes of the particle. Our dbcc crystal is close to the predicted O_1 crystal, whose lattice vectors are $\boldsymbol{e}_1 = 0.912492\boldsymbol{i} + 0.912492\boldsymbol{j} - 0.912492\boldsymbol{k}$, $\boldsymbol{e}_2 = -0.2884\boldsymbol{i} + 1.80629\boldsymbol{j} - 0.2884\boldsymbol{k}$, and $\boldsymbol{e}_3 = 0.2884\boldsymbol{i} - 0.2884\boldsymbol{j} - 1.80629\boldsymbol{k}$. However, it has a packing fraction of $\phi = 0.832839$ which is denser than the predicted O_1 crystal with $\phi = 0.824976$ in ref. 10 and 11 by roughly 1%. In ref. 10 and 11, the O_0 and O_1 phases are found to switch at $q = 0.79248$. We also observed that both the bct and dbcc crystals transform into the bcc phase at $q = 0.79248$.

As shown in Fig. 3, when the shape of the superballs is close to spherical, *i.e.*, $0.7 < q < 3$ corresponding to an asphericity $A \lesssim 0.08$ for cube-like and $A \lesssim 0.03$ for octahedron-like superballs, there is always a stable fcc plastic crystal phase. Surprisingly, when the shape of superballs is octahedron-like, we find a stable bcc plastic crystal phase. Moreover, around $q = 0.8$ we even find a fairly broad two-phase regime where a low-density fcc plastic crystal coexists with a high-density bcc plastic crystal phase. In order to quantify the orientational order in the bcc plastic crystal, we calculate the cubic order parameter S_4 given by:[12]

$$S_4 = \max_{\boldsymbol{n}} \left\{ \frac{1}{14N} \sum_{i,j} \left(35 |\boldsymbol{u}_{ij} \cdot \boldsymbol{n}|^4 - 30 |\boldsymbol{u}_{ij} \cdot \boldsymbol{n}|^2 + 3 \right) \right\}, \quad (10)$$

where $\boldsymbol{u}_{ij}$ is the unit vector of the j^{th} axis of particle i, N is the number of particles, and $\boldsymbol{n}$ is a unit vector. The cubic order

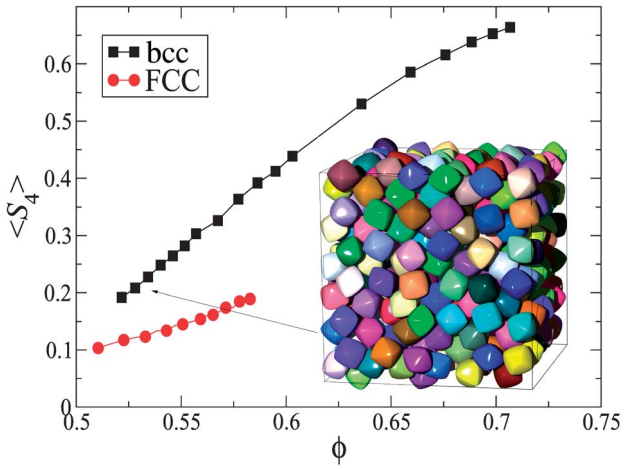

Fig. 4 Cubic order parameter S_4 as a function of packing fraction ϕ for a bcc and a (metastable) fcc plastic crystal phase of hard superballs with $q = 0.7$. The inset shows a typical configuration of a BCC plastic crystal of hard superballs with $q = 0.7$ at $\phi = 0.54$.

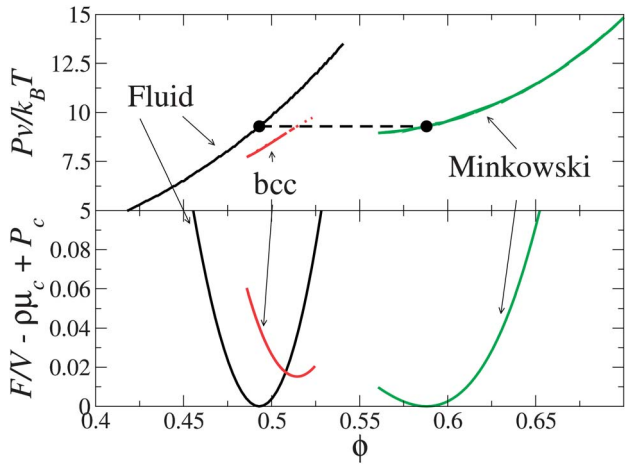

Fig. 5 A part of the equation of state for hard octahedra. The pressure Pv/k_BT and free-energy density $F/V - \rho\mu_c + P_c$ as a function of packing fraction ϕ. Here v is the volume of the particle; F and V are the Helmholtz free energy and the volume of the system (in units of particle volume) respectively; μ_c and P_c are the chemical potential and pressure at bulk coexistence respectively with ρ the number density of the particles. The solid lines in the EOS for the Minkowski and the bcc plastic crystal phases are obtained by melting the close-packed Minkowski crystal in floppy-box *NPT* MC simulations, and the dotted line for the bcc plastic crystal is obtained by compressing the crystal in cubic box *NPT* MC simulations. The black points and dashed line show the coexistence between the fluid phase and the Minkowski crystal phase.

parameter S_4 is shown in Fig. 4 as a function of packing fraction for the bcc plastic crystal phase of superballs with $q = 0.7$. For comparison, we also show S_4 for the (metastable) fcc plastic crystal phase for which the cubic order is always very low $\langle S_4 \rangle \lesssim 0.2$. We observe that $\langle S_4 \rangle \lesssim 0.2$ at low packing fractions, which means that there is a very weak orientational order in the system.[28] With increasing packing fraction, the cubic order parameter increases monotonically to around 0.65 at a packing fraction of 0.7, which is indicative of a medium-ranged orientationally ordered system. This suggests that the entropic repulsion due to the rotation of the octahedron-like superballs stabilizes the bcc lattice. Moreover, as a bcc-like phase is the best-packed crystal structure for these superballs, the translational entropy gained in the bcc rotator phase outweighs the loss in orientational entropy compared to the fcc rotator phase at the same packing fraction.

Due to the numerical instability in the overlap algorithm, we are not able to investigate systems of superballs with $q < 0.7$.[24] However, we can use the separating axis theorem[6] to simulate hard superballs with $q = 0.5$, *i.e.*, perfect octahedra. When we compressed the system from a fluid phase, we did not observe the spontaneous formation of a crystal phase in our simulation box within our simulation time. When we expand the Minkowski crystal, which is the close-packed structure of octahedra, in *NPT* MC simulations by decreasing the pressure, the system melts into a bcc plastic crystal phase as shown in Fig. 5. We also calculated the free energy for these three phases to determine the phase boundaries. To exclude finite-size effects in the free-energy calculation of crystal phases, we performed Einstein integration for systems of $N = 1024$, 1458, and 2000 particles, and applied a finite-size correction.[23] Also see Appendix A.3 and Fig. 9 for this procedure. We confirmed the errors in the free-energy calculations to be on the order of $10^{-3}k_BT$ per particle. The calculated free-energy densities for the three phases are shown in Fig. 5. Employing a common tangent construction, we found that there is only phase coexistence between a fluid phase and a Minkowski crystal phase, while the bcc plastic crystal phase is metastable. Moreover, the Minkowski crystal melts into a bcc plastic crystal before melting into the fluid phase. Our results thus show that the rounded corners of octahedra play an important role in stabilizing the bcc plastic crystal phase. We note here that stable bcc rotator phases have been reported before for soft particles, *e.g.*, for simple water models[29] and SF_6 molecules with an octagonal shape.[30] However, its stability for systems of hard particles has not been demonstrated before to the best of our knowledge.

4. Conclusion

In conclusion, using free-energy calculations we have determined the full phase diagram of hard superballs with shapes interpolating between cubes and octahedra, *i.e.*, $0.5 \leq q < \infty$. In systems of cube-like superballs ($q > 1$), we find a stable deformed C_1 phase at high packing fraction, except close to the sphere-limit ($q = 1$) where a deformed C_0 crystal is stable. For $q < 3$ the crystal phase melts into a fcc plastic crystal before melting into a fluid phase of cube-like superballs. In systems of octahedron-like superballs ($0.5 < q < 1$), we find a stable bct or a deformed bcc crystal phase upon approaching close packing, with a crossover at $q = 0.79248$. Moreover, a stable fcc plastic crystal appears at intermediate densities for $0.7 < q \leq 1$. Interestingly, for $q < 0.85$, we find a novel stable bcc plastic crystal phase, which can even coexist with the fcc plastic crystal phase at around $q = 0.8$. It is worth noting that phase coexistence between a bcc and a fcc plastic crystal phase has been predicted for particles interacting with soft potentials, *e.g.*, for simple water models.[29] More surprisingly, the bcc and fcc rotator phases are unstable for the flat-faced and sharp-edged hard octahedra and hard cubes, respectively, which suggests that the asphericity A as defined in eqn (2) and the curvature of superballs may play an important

role in stabilizing rotator phases. As the asphericity A increases smoothly by deviating from $q = 1$, as shown in Fig. 1, it is hard to define a stability criterion for the plastic crystal phases based on a threshold value of A. However, we find stable rotator phases for the shape parameter range $0.7 < q < 3$, which corresponds to an asphericity $A \lesssim 0.08$ for cube-like and $A \lesssim 0.03$ for octahedron-like superballs. In addition, we determine the total and local Gaussian curvature for the superballs in Appendix A.4. The total Gaussian curvature of a superball equals 4π independent of the shape parameter q and in agreement with the Gauss–Bonnet theorem. In Fig. 10, we show the distribution of local curvature K on the surface of various superballs. We observe that for the stability range of the rotator phases $0.7 < q < 3$, the variations in the distribution of the local curvature on the superball are relatively moderate. For particles that display regions with high curvature (sharp edges) and simultaneously regions with no curvature (flat faces) the rotator phases are destabilized. Hence, one may argue that entropic directional forces[19] that tend to align sufficiently large flat faces of polyhedral-shaped particles destabilize rotator phases in favor of crystals. We stress here that rounded corners are not a necessary condition for stable rotator phases since almost spherical polyhedral particles have been shown to form rotator phases as well.[6] Finally, we also observed a two-step melting phenomenon in a system of hard octahedra, such that the Minkowski crystal melts into a metastable bcc plastic crystal before melting into the fluid phase. Nanoparticle self-assembly is therefore surprisingly sensitive to the particle curvature.

A Appendix

A.1 Overlap algorithm for superballs

The algorithm we used to check for overlaps between superballs is based on the Perram and Wertheim (PW) potential introduced in ref. 31. The details of the application of this general method to the specific case of superballs can be found in ref. 24. A superball with shape parameter q, located at $\boldsymbol{r}_0$, and orientation matrix $\boldsymbol{O} = (\boldsymbol{o}_1,\boldsymbol{o}_2,\boldsymbol{o}_3)$ is given by the set of points $\{\boldsymbol{r}|\zeta(\boldsymbol{r}) \leq 0, \boldsymbol{r} \in \mathbb{R}^3\}$ with ζ an appropriate shape function. The shape function is strictly convex and defined by

$$\zeta(\boldsymbol{r}) = g[\tilde{\zeta}(\tilde{\boldsymbol{r}})] - 1 \tag{11}$$

with

$$g(x) = x^{1/q}$$

$$\tilde{\zeta}(\tilde{\boldsymbol{r}}) = \tilde{r}_1^{2q} + \tilde{r}_2^{2q} + \tilde{r}_3^{2q}$$

where $\tilde{\boldsymbol{r}} = (\tilde{r}_1,\tilde{r}_2,\tilde{r}_3)^T = \boldsymbol{O}^{-1}(\boldsymbol{r} - \boldsymbol{r}_0)$ gives the relative coordinates of $\boldsymbol{r}$ with respect to the particle centered at $\boldsymbol{r}_0$ with the reference orientation $\boldsymbol{O}$.

The condition for overlap between a pair of particles A and B can be thought of as an inequality between the position and orientation of the particles. For this purpose, we measure the distance between the two superballs using the overlap potential ζ(A,B), where A and B contain the information for the location and orientation of the two superballs. The sign of ζ(A,B) gives us an overlap criterion through

$$\begin{cases} \zeta(\mathrm{A},\mathrm{B}) > 0 & \text{if A and B are disjoint} \\ \zeta(\mathrm{A},\mathrm{B}) = 0 & \text{if A and B are externally tangent} \\ \zeta(\mathrm{A},\mathrm{B}) < 0 & \text{if A and B are overlapping} \end{cases} \tag{12}$$

ζ(A,B) is also at least twice continuously differentiable in the position and orientation of A and B, respectively.

In the following we describe the procedure by which ζ(A,B) can be determined for two superballs with given position and orientation. We define and compute the overlap conditions using a procedure originally developed for ellipsoids by Perram and Wertheim.[31] The PW overlap potential is defined by

$$\zeta(\mathrm{A},\mathrm{B}) = \max_{0 \leq \lambda \leq 1} \min_{\boldsymbol{r}_C} \left[\lambda\zeta_A(\boldsymbol{r}_C) + (1-\lambda)\zeta_B(\boldsymbol{r}_C)\right], \tag{13}$$

where $\zeta_A(\boldsymbol{r}_C)$ and $\zeta_B(\boldsymbol{r}_C)$ are the shape functions that define the two superballs A and B, respectively. Here $\boldsymbol{r}_C$ can be thought of as the first point of contact between A and B, when these particles are uniformly expanded/scaled, whilst keeping their orientation and position fixed. This is illustrated in Fig. 6.

For every λ, the solution of the inner optimization over $\boldsymbol{r}_C$ is unique due to the strict convexity of A and B, and it satisfies the gradient condition

$$\nabla\zeta(\mathrm{A},\mathrm{B}) = \lambda\nabla\zeta_A(\boldsymbol{r}_C) + (1-\lambda)\nabla\zeta_B(\boldsymbol{r}_C), \tag{14}$$

which shows that the normal vectors are anti-parallel as shown in Fig. 6. The solution of the outer optimization problem over λ is specified by the condition

$$\zeta(\mathrm{A},\mathrm{B}) = \zeta_A(\boldsymbol{r}_C) = \zeta_B(\boldsymbol{r}_C). \tag{15}$$

Calculation of the PW overlap potential can be done by solving for $\boldsymbol{r}_C(\lambda)$ in eqn (14), and then determining the λ that satisfies eqn (15). The solution to eqn (13) can be obtained by solving a set of ordinary differential equations (ODEs) and by making use of the ODE event location method[32] to achieve $\zeta_A(\boldsymbol{r}_C) = \zeta_B(\boldsymbol{r}_C)$. This method is rigorous in the sense that the optimal λ can be determined within an arbitrary accuracy, however, it is inefficient since it requires solving ODEs.

If a good-enough initial guess can be provided for λ, one can directly use the Newton–Raphson (NR) method on this system of two equations. The method has the advantage that it is more

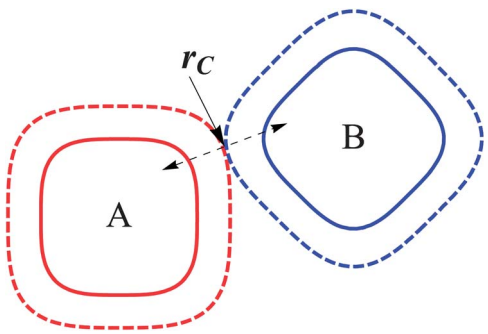

Fig. 6 An illustration of the scaling procedure applied to the two superballs A and B, which results in the contact point at $\boldsymbol{r}_C$, and the two anti-parallel vectors that are normal to the scaled surfaces of the particles at $\boldsymbol{r}_C$.

Table 2 Helmholtz free energy per particle, $F(\rho_0)/Nk_BT$, for the crystal phases of hard superballs with various shape parameter values q at density ρ_0 as calculated using the Einstein-integration method. Here fcc, bcc, and bct are the abbreviations for the face-centered cubic, body-centered cubic, and body-centered tetragonal crystal phases, respectively. The C_1 crystal is defined in the main text and in ref. 10

q	Crystal type	N	$\rho_0 a^3$	$F(\rho_0)/Nk_BT$
0.70000	Plastic bcc	512	0.21200	4.22893
0.70000	Plastic fcc	500	0.21200	4.27468
0.79248	Plastic bcc	512	0.17589	3.80535
0.79248	Plastic fcc	500	0.17589	3.67894
0.85000	Plastic fcc	500	0.17189	4.45765
0.85000	Plastic bcc	432	0.17189	4.84055
0.85000	bct	512	0.20716	11.9065
1.75000	Deformed C_1	512	0.11654	9.42461
1.75000	Plastic fcc	500	0.09760	4.54847
2.50000	Deformed C_1	512	0.10675	9.58457
2.50000	Plastic fcc	500	0.07700	3.13303
3.00000	Deformed C_1	512	0.10522	10.0684
3.00000	Plastic fcc	500	0.07600	3.77605

efficient than the one used in ref. 32. The Newton–Raphson steps are determined as follows

$$\Delta\lambda = \frac{-1}{\zeta_{\lambda\lambda}}\left[(\zeta_B - \zeta_A) - \Delta \boldsymbol{g}^T \boldsymbol{M}^{-1} \nabla\zeta_{AB}\right], \tag{16}$$

$$\Delta \boldsymbol{r}_C = \boldsymbol{M}^{-1}(\Delta \boldsymbol{g}\Delta\lambda - \nabla\zeta_{AB}), \tag{17}$$

where

$$\boldsymbol{M} = \lambda\nabla^2\zeta_A + (1-\lambda)\nabla^2\zeta_B,$$

$$\Delta \boldsymbol{g} = \nabla\zeta_A - \nabla\zeta_B,$$

$$\zeta_{\lambda\lambda} = \Delta \boldsymbol{g}^T \boldsymbol{M}^{-1} \Delta \boldsymbol{g},$$

$$\nabla\zeta(\boldsymbol{r}_C) = g'[\tilde{\zeta}(\tilde{\boldsymbol{r}}_C)]\nabla\tilde{\zeta}(\tilde{\boldsymbol{r}}_C),$$

$$\nabla^2\zeta(\boldsymbol{r}_C) = g'[\tilde{\zeta}(\tilde{\boldsymbol{r}}_C)](\nabla^2\tilde{\zeta}(\tilde{\boldsymbol{r}}_C)) + g''[\tilde{\zeta}(\tilde{\boldsymbol{r}}_C)](\nabla\tilde{\zeta}(\tilde{\boldsymbol{r}}_C))(\nabla\tilde{\zeta}(\tilde{\boldsymbol{r}}_C))^T,$$

$$\nabla\tilde{\zeta}(\tilde{\boldsymbol{r}}_C) = \boldsymbol{O}\nabla_{\tilde{\boldsymbol{r}}_C}\tilde{\zeta}(\tilde{\boldsymbol{r}}_C),$$

$$\nabla^2\tilde{\zeta}(\tilde{\boldsymbol{r}}_C) = \boldsymbol{O}\nabla_{\tilde{\boldsymbol{r}}_C}{}^2\tilde{\zeta}(\tilde{\boldsymbol{r}}_C)\boldsymbol{O}^T,$$

with $\boldsymbol{O}$ an orthogonal matrix, and $\nabla_{\tilde{\boldsymbol{r}}_C}$ and $\nabla_{\tilde{\boldsymbol{r}}_C}{}^2$ the gradient and Hessian matrix with respect to $\tilde{\boldsymbol{r}}_C$, respectively. Here we also corrected the typographical errors in ref. 24.

We have found that this NR method is only sufficiently numerically stable for simulations of superballs with $0.85 \leq q \leq 1.7$. Therefore, in order to improve the range of stability, we make the following modifications to the Newton–Raphson steps:

$$\Delta\lambda^* = \frac{\Delta\lambda\cdot\alpha}{\max(|\Delta\lambda|, |\Delta\boldsymbol{r}_C|)} \tag{18}$$

$$\Delta\boldsymbol{r}_C^* = \frac{\Delta\boldsymbol{r}_C\cdot\alpha}{\max(|\Delta\lambda|, |\Delta\boldsymbol{r}_C|)} \tag{19}$$

where α is a uniform random number in interval [0,1). Essentially the modification makes the length of Newton–Raphson steps randomly smaller than unity. This helps to avoid the divergence of the iterations in the NR procedure around singularities. With this modification, we have shown that we are able to study systems of superballs with $0.7 \leq q \leq 3.5$.

A.2 Free energies and equations of state for hard superballs

In this section, we give the free energies of the fluid phase (Table 1) and the crystal phases (Table 2) used to construct the phase diagram in Fig. 3. We also give several equations of state in Fig. 7 and 8 for the corresponding phases. Note that the exact value of free energy depends on the unit of length; here we set the radius of the superball $a = 1$.

A.3 Finite size scaling for the free energies of hard octahedra

The excess free energy density as a function of $1/N$ for systems of hard octahedra in a Minkowski crystal and in a bcc plastic crystal phase is shown in Fig. 9. After finite-size scaling the Helmholtz free energy per particle in a Minkowski crystal ($\phi = 0.71052$) and

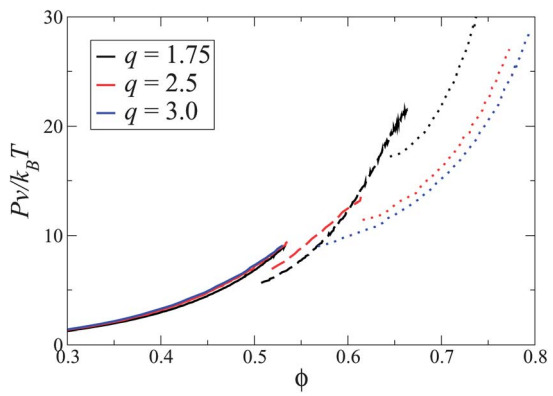

Fig. 7 Equation of state for cube-like hard superballs with various shape parameters q. The solid, dashed, and dotted lines indicate the fluid, plastic fcc, and deformed C_1 phases, respectively. P and ϕ denote the pressure and packing fraction of the system, and v is the volume of a particle. The color of the lines gives the shape (parameter q) of the particles.

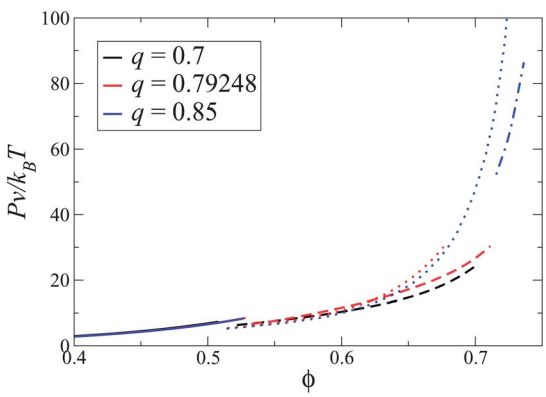

Fig. 8 Equation of state for octahedron-like hard superballs with various shape parameters q. The solid, dashed, dotted, and dash-dotted lines indicate the fluid, plastic bcc, plastic fcc, and bct phases, respectively. P and ϕ denote the pressure and packing fraction of the system, and v is the volume of a particle. The color of the lines gives the shape (parameter q) of the particles.

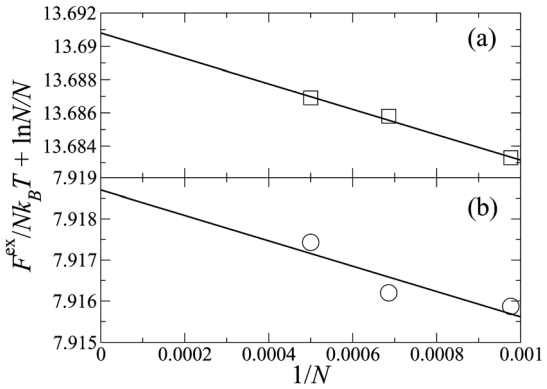

Fig. 9 $F^{ex}/Nk_BT + \ln N/N$ as a function of $1/N$ for a system of hard octahedra in a Minkowski crystal (a) and in a bcc plastic crystal phase (b) at packing fraction $\phi = 0.71052$ and 0.5, respectively.

in a bcc plastic-crystal phase ($\phi = 0.5$) is $12.349159k_BT$ and $6.22587k_BT$, respectively. Note that in these calculations we used the volume of an octahedron as the unit volume.

A.4 Local geometric properties of superballs

To show the geometric properties of a superball as defined in eqn (1), we derive the local Gaussian curvature of this object. To that end we parameterize the points (x,y,z) on the surface of a superball with shape parameter q as

$$\begin{cases} x = |\cos\varphi|^{1/q}|\cos\theta|^{1/q}\cdot\mathrm{sign}(\cos\varphi)\cdot\mathrm{sign}(\cos\theta) \\ y = |\cos\varphi|^{1/q}|\sin\theta|^{1/q}\cdot\mathrm{sign}(\cos\varphi)\cdot\mathrm{sign}(\sin\theta) \\ z = |\sin\varphi|^{1/q}\cdot\mathrm{sign}(\sin\varphi) \end{cases}, \quad (20)$$

where $-\pi/2 \le \varphi \le \pi/2$ and $-\pi \le \theta \le \pi$ are the polar and azimuthal angles, respectively. Then the local Gaussian curvature K at a point (x,y,z) is given by

$$K = \frac{K_1}{(K_2 + K_3)^2}, \quad (21)$$

where

$$K_1 = (2q-1)^2\cos^{2+2/q}\theta\cos^4\varphi\sin^{2+2/q}\theta\sin^{2+2/q}\varphi;$$

$$K_2 = \cos^{2/q}\theta\cos^{2/q}\varphi\sin^{2/q}\theta\sin^4\varphi;$$

$$K_3 = \cos^4\varphi\sin^{2/q}\varphi(\cos^{2/q}\theta\sin^4\theta + \cos^4\theta\sin^{2/q}\theta),$$

with $0 \le \varphi \le \pi/2$ and $0 \le \theta \le \pi/2$.

One can show by integration that the total Gaussian curvature of a superball is given by

$$\iint_{|x|^{2q}+|y|^{2q}+|z|^{2q}=1} K\,\mathrm{d}\boldsymbol{S} = 4\pi, \quad (22)$$

which is in agreement with the Gauss–Bonnet theorem. Moreover, as shown in Fig. 10, the distribution of the local curvature on the surface of a superball has strongly pronounced peaks at

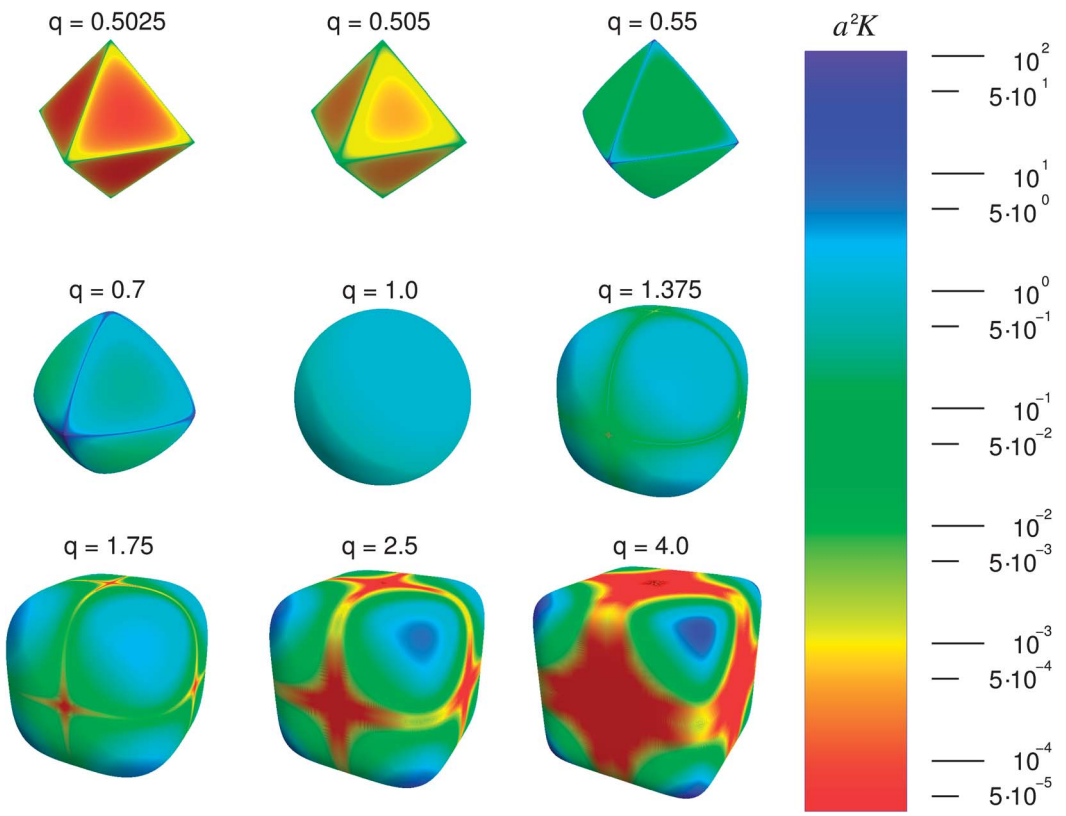

Fig. 10 The distribution of the local Gaussian curvature K on the surface of superballs for various choices of the shape parameter q. Here $a = 1$ is the radius of the particle. Red indicates the regions where the particle is (almost) flat and blue indicates the regions with high curvature. Note that our free-energy calculations predict stable rotator phases for the superballs with $q = 0.7$, 1.0, 1.375, 1.75, and 2.5.

the corners of the particle, which suggests that both the flat faces and the rounding of the corners may play a dominant role in the way that the phase behavior changes with varying shape parameter.

Acknowledgements

We thank Dr F. Smallenburg for fruitful discussions and Dr D. Ashton for making the snapshot in Fig. 4. We acknowledge the financial support from a NWO-VICI grant and Utrecht University High Potential Programme.

References

1 S. C. Glotzer and M. J. Solomon, *Nat. Mater.*, 2007, **6**, 557.
2 A. Yethiraj and A. van Blaaderen, *Nature*, 2003, **421**, 513.
3 Y. Zhang, F. Lu, D. van der Lelie and O. Gang, *Phys. Rev. Lett.*, 2011, **107**, 135701.
4 A.-P. Hynninen, J. H. J. Thijssen, E. C. M. Vermolen, M. Dijkstra and A. van Blaaderen, *Nat. Mater.*, 2007, **6**, 202.
5 A. Haji-Akbari, M. Engel, A. S. Keys, X. Zheng, R. G. Petschek, P. Palffy-Muhoray and S. C. Glotzer, *Nature*, 2009, **462**, 773.
6 U. Agarwal and F. Escobedo, *Nat. Mater.*, 2011, **10**, 230.
7 S. Torquato and Y. Jiao, *Nature*, 2009, **460**, 876.
8 T. C. Hales and S. P. Ferguson, *Discrete Comput. Geom.*, 2006, **36**, 5.
9 J. de Graaf, R. van Roij and M. Dijkstra, *Phys. Rev. Lett.*, 2011, **107**, 155501.
10 Y. Jiao, F. H. Stillinger and S. Torquato, *Phys. Rev. E: Stat., Nonlinear, Soft Matter Phys.*, 2009, **79**, 041309.
11 Y. Jiao, F. H. Stillinger and S. Torquato, *Phys. Rev. E: Stat., Nonlinear, Soft Matter Phys.*, 2011, **84**, 069902.
12 R. D. Batten, F. H. Stillinger and S. Torquato, *Phys. Rev. E: Stat., Nonlinear, Soft Matter Phys.*, 2010, **81**, 061105.
13 M. Marechal, A. Cuetos, B. Martínez-Haya and M. Dijkstra, *J. Chem. Phys.*, 2011, **134**, 094501.
14 F. Smallenburg, L. Filion, M. Marechal and M. Dijkstra, 2011, arXiv:1111.3466v2 [cond–mat.soft], submitted.
15 C. Vega and P. A. Monson, *J. Chem. Phys.*, 1997, **107**, 2696.
16 M. Marechal and M. Dijkstra, *Phys. Rev. E: Stat., Nonlinear, Soft Matter Phys.*, 2008, **77**, 061405.
17 P. Bolhuis and D. Frenkel, *J. Chem. Phys.*, 1997, **106**, 666.
18 P. G. Bolhuis, D. Frenkel, S.-C. Mau and D. A. Huse, *Nature*, 1997, **388**, 235.
19 P. F. Damasceno, M. Engel and S. C. Glotzer, *ACS Nano*, 2012, **6**, 609.
20 L. Rossi, S. Sacanna, W. T. M. Irvine, P. M. Chaikin, D. J. Pine and A. P. Philipse, *Soft Matter*, 2011, **7**, 4139.
21 W. L. Miller and A. Cacciuto, *J. Chem. Phys.*, 2010, **133**, 234903.
22 W. L. Miller, B. Bozorgui and A. Cacciuto, *J. Chem. Phys.*, 2010, **132**, 134901.
23 D. Frenkel and B. Smit, *Understanding Molecular Simulation: From Algorithms to Applications*, Academic Press, 2002.
24 A. Donev, PhD thesis, Princeton University, 2006.
25 A. Fortini, M. Dijkstra, M. Schmidt and P. P. F. Wessels, *Phys. Rev. E: Stat., Nonlinear, Soft Matter Phys.*, 2005, **71**, 051403.
26 L. Filion, M. Marechal, B. van Oorschot, D. Pelt, F. Smallenburg and M. Dijkstra, *Phys. Rev. Lett.*, 2009, **103**, 188302.
27 H. Minkowski, Königliche Gesellschaft der Wissenschaften zu Göttingen, Math.-Phys. KL (1904), 1904, 311–355.
28 See ESI† for the movieof the plastic bcc crystal formed by superballs with $q = 0.7$ at packing fraction 0.54.
29 J. L. Aragones and C. Vega, *J. Chem. Phys.*, 2009, **130**, 244504.
30 J.-M. Leyssale, J. Delhommelle and C. Millot, *J. Chem. Phys.*, 2007, **127**, 044504.
31 J. W. Perram and M. Wertheim, *J. Comput. Phys.*, 1985, **58**, 409–416.
32 L. F. Shampine, I. Gladwell and R. W. Brankin, *Assoc. Comput. Mach., Trans. Math. Software*, 1991, **17**, 11–25.

